

Search for Light Dark Sectors Using Electron-Photon Collisions

L. Angel^{a,b,c,d,1} **G. Casse**^{e,f} **G. Gambini**^g **A. S. de Jesus**^h **V. Kozhuharov**^{i,j} **A. Machado**^k **F. S. Queiroz**^{a,b,l,m} **E. Segreto**^k **J. Smirnov**^f

^a*Departamento de Física, Universidade Federal do Rio Grande do Norte, 59078-970, Natal, RN, Brasil*

^b*International Institute of Physics, Universidade Federal do Rio Grande do Norte, Campus Universitario, Lagoa Nova, Natal-RN 59078-970, Brazil*

^c*Department of Physics, University of Oslo, Box 1048, N-0316 Oslo, Norway*

^d*Max Planck Institut für Kernphysik, Heidelberg, Germany*

^e*Oliver Lodge Laboratory, University of Liverpool, Liverpool L69 7ZE, United Kingdom*

^f*Department of Mathematical Sciences, University of Liverpool, Liverpool, L69 7ZL, United Kingdom*

^g*Facultad de Ciencias, Universidad Nacional de Ingeniería (UNI), Av. Túpac Amaru 210, Lima, Perú*

^h*Departamento de Física Matemática, Instituto de Física, Universidade de São Paulo, 05315-970 São Paulo, Brasil*

ⁱ*Faculty of Physics, Sofia University, 5 J. Bourchier Blvd., 1164 Sofia, Bulgaria*

^j*INFN - LNF, Via E. Fermi 54 - 00044 Frascati, Italy*

^k*Instituto de Física “Gleb Wataghin”, Universidade Estadual de Campinas (UNICAMP), Rua Sérgio Buarque de Holanda 777, CEP 13083-859, Campinas, São Paulo, Brazil*

^l*Millennium Institute for Subatomic Physics at the High-Energy Frontier (SAPHIR) of ANID, Fernández Concha 700, Santiago, Chile*

^m*Universidad de La Serena, Avenida Cisternas 1200, La Serena, Chile*

E-mail: lucia.correa.717@ufrn.edu.br, venelin.kozhuharov@cern.ch, farinaldo.queiroz@ufrn.edu.br

ABSTRACT: The dark photon is a new gauge boson that naturally arises in many beyond the Standard Model theoretical models, featuring interactions that resemble quantum electrodynamics. Due to this feature, it is often considered the portal between dark and visible sectors. For this reason, it has become the target of many experimental searches worldwide. In this work, we propose a search for dark photons based on the Inverse Compton scattering, $\gamma e^- \rightarrow A' e^-$, to be conducted at electron accelerators. In this setup, photons from a laser source would impinge on the accelerated electron beam, producing a dark photon in the final state. We propose an experimental setup to take advantage of the photon counting technique, and we derive the projected sensitivity by considering the energy of the incident photon to be about 1 eV and an electron beam of 3 GeV. We show that this experimental setup could cover an unexplored region of parameter space and constitute a promising probe for dark sectors in the future.

¹Corresponding author.

Contents

1	Introduction	1
2	Dark Photon Model	2
3	Current Status of Experimental Searches	3
4	The Dark Inverse Compton Scattering	6
5	Experimental Setup	9
6	Lower Photon Detection Thresholds	12
7	Discussion	14
	7.1 Background	14
	7.2 Projected Sensitivity	14
8	Conclusions	16
A	Energy distribution of the electron in DICS process	18
B	Flux of Dark Photons as a Function of the Scattering Angle ϕ	18

1 Introduction

The Standard Model (SM) of particle physics constitutes a successful theoretical framework that describes three of the four known interactions in nature: the strong, weak, and electromagnetic interactions. However, there are numerous phenomena for which the SM is unable to provide a reasonable description. One of these phenomena is dark matter (DM), whose existence has been a subject of interest for many decades due to multiple pieces of evidence of its gravitational interaction, such as the observed versus expected matter discrepancy in the Coma Cluster, documented by Fritz Zwicky [1]; the rotation curve of galaxies, later observed by Vera Rubin and Kent Ford [2]; the distribution of anisotropies in the cosmic microwave background (CMB) [3]; the collision system of the Bullet Cluster [4]; the formation of large-scale structures [5]; and the amount of baryonic matter inferred by Big Bang nucleosynthesis (BBN) [6], which is insufficient to explain the fluctuations in the Cosmic Microwave Background (CMB), among others.

The mere evidence of the existence of DM provides a strong indication that a dark sector beyond the known fundamental forces could exist [7–10]. Given that the SM can only account for a small fraction of the universe (approximately 5% of it consisting of baryonic matter), it is not surprising to consider the possibility of the existence of a rich and still

undiscovered dark sector filled with exotic particles, which are entitled to interesting signatures. This dark sector, often referred to as the “hidden” sector in the literature, could contain the so-called light and weakly coupled particles, which, as the name suggests, would interact very weakly with the known particles of the SM. In this project, the focus will be directed towards the study of the dark photon, which is a sort of a massive photon with electromagnetic interactions similar to the photon. The presence of new vector field with such properties is considered to be the simplest extension beyond the Standard Model. Due to its simplicity and resemblance to quantum electrodynamics, it has been the target of a multitude of experimental searches going from direct production at low-energy accelerators to astrophysical probes. In this work, we propose to take advantage of low-energy electron accelerators to access new physics at much lower energy scales using lasers. In this work, we will focus on the dark photon model. We propose here a collision between an electron beam and a photon from a laser, which could produce dark photons through an Inverse Compton process (ICS) $\gamma e^- \rightarrow A' e^-$ covering a different mass range from previous dark photon related proposal [11–15]. Generally speaking, this electron-photon collision can be applied to existing electron accelerators, but the experimental setup and physics scale involved depend very much on the technical details. In other words, the new physics reach can be determined once some accelerator parameters are laid out. That said, for concreteness, we will concentrate our discussion on 3 GeV electron beams existing at the Sirius accelerator [16, 17]. This article is organized as follows: In Section 2, we present some of the characteristics of the dark photon model, where we review its features and different kinds of searches. Section 3 covers the current status of the experimental searches for dark photons in the different contexts, from Helioscopes to DM direct search experiments. Section 5 is devoted to our proposal, which shows the setup of the precision experiment using Sirius and presents the results and parameter space covered by our proposition. We continue with Section 7 with a discussion about the obtained results and the implications of indirectly probing dark photons. The conclusions are given in Section 8.

2 Dark Photon Model

The dark photon (DP), also known as the hidden photon or heavy photon and typically denoted as A' , γ' , or U , was first proposed by Bob Holdom [18] in the context of a model featuring an additional renormalizable $U(1)_\chi$ local symmetry group [19]. In this framework, the dark photon mixes with the SM neutral gauge bosons through a kinetic mixing term, with the mixing represented by the parameter ε , which is usually considered to be small ($\varepsilon \ll 1$). This mixing establishes a portal between the SM and the dark sector, potentially allowing interactions between dark matter and visible matter [20]. The dark photon could also be a viable candidate for bosonic dark matter, however, in this paper we only consider it as a mediator between DM and SM particles.

There are two types of dark photons: massive and massless, similar to the SM photon. However, the focus of the community is on the massive case, as its direct current-like coupling to ordinary matter could facilitate detection [20, 21]. Therefore, the free parameters of the model are the kinetic mixing ε and the dark photon mass $m_{A'}$.

The Lagrangian that describes the mixing between the SM photon and the vector boson of the new gauge symmetry is given by:

$$\mathcal{L} = -\frac{\varepsilon}{2}F_{\mu\nu}\chi^{\mu\nu}, \quad (2.1)$$

where ε is the free parameter known as “kinetic mixing”, $F_{\mu\nu}$ is the electromagnetic strength tensor, and χ is the strength tensor for the new interaction mediated by the dark photon. This work assumes that the dark photon has mass, which can be acquired through the Stueckelberg mechanism [22, 23] or via spontaneous symmetry breaking of the gauge symmetry [24]. The mixing implies that none of the gauge bosons are physical, thus requiring diagonalization of the fields. After diagonalization, the Lagrangian that describes the interaction of the dark photon with the electromagnetic current of the SM can finally be expressed as:

$$\mathcal{L} \supset -\frac{e\varepsilon}{\sqrt{1-\varepsilon^2}}J_\mu A'^\mu \simeq -e\varepsilon J_\mu A'^\mu. \quad (2.2)$$

3 Current Status of Experimental Searches

Since the DP couples to the electromagnetic current in a manner analogous to the SM photon, its production mechanisms mirror those of ordinary photons. The primary production channels include Bremsstrahlung ($e^-Z \rightarrow e^-ZA'$), annihilation ($e^-e^+ \rightarrow \gamma A'$), Drell-Yan ($q\bar{q} \rightarrow A' \rightarrow l^+l^-$ or h^+h^-), meson decays ($M \rightarrow \gamma A'$) and inverse Compton-like process ($e^-\gamma \rightarrow e^-A'$), which constitutes the main focus of this work.

Based on the different production mechanisms, various experiments have been developed using different techniques, primarily centered on the decay modes (visible or invisible), depending on the mass range and experimental properties. The following will briefly outline each of the sources of the current experimental constraints on the mass of the dark photon and the kinetic mixing parameter ε for $m_{A'} < 1$ MeV, which is our region of interest:

- *Light Shining through Walls (LSW) & Helioscopes*: LSW is an experimental method used in the search for Beyond the Standard Model (BSM) particles, particularly Weakly Interacting Sub-eV Particles (WISPs), taking advantage of their possible mixing with the SM photon [25]. This method was first proposed in 1982 [7] to search for dark photons. It was later adapted to explore axion-like particles [26, 27]. The method involves directing a high-power laser through a region with a strong magnetic field. The interaction between the photons and the magnetic field can generate a beam of new particles. Unlike the original laser beam, these particles may be capable of passing through a solid barrier (e.g., a wall). After passing through the barrier, a second magnetic field of comparable strength redirects the newly produced particles toward a detector [25, 28]. In the case of helioscopes, their setup consists of a long, sealed cavity that points toward the Sun. Inside this cavity, a powerful magnetic field is generated. At the end of the cavity, there is an X-ray detector sensitive to weak signals. Originally, the magnetic field was introduced to facilitate the oscillation of axions into photons. However, the setup can be adapted for the

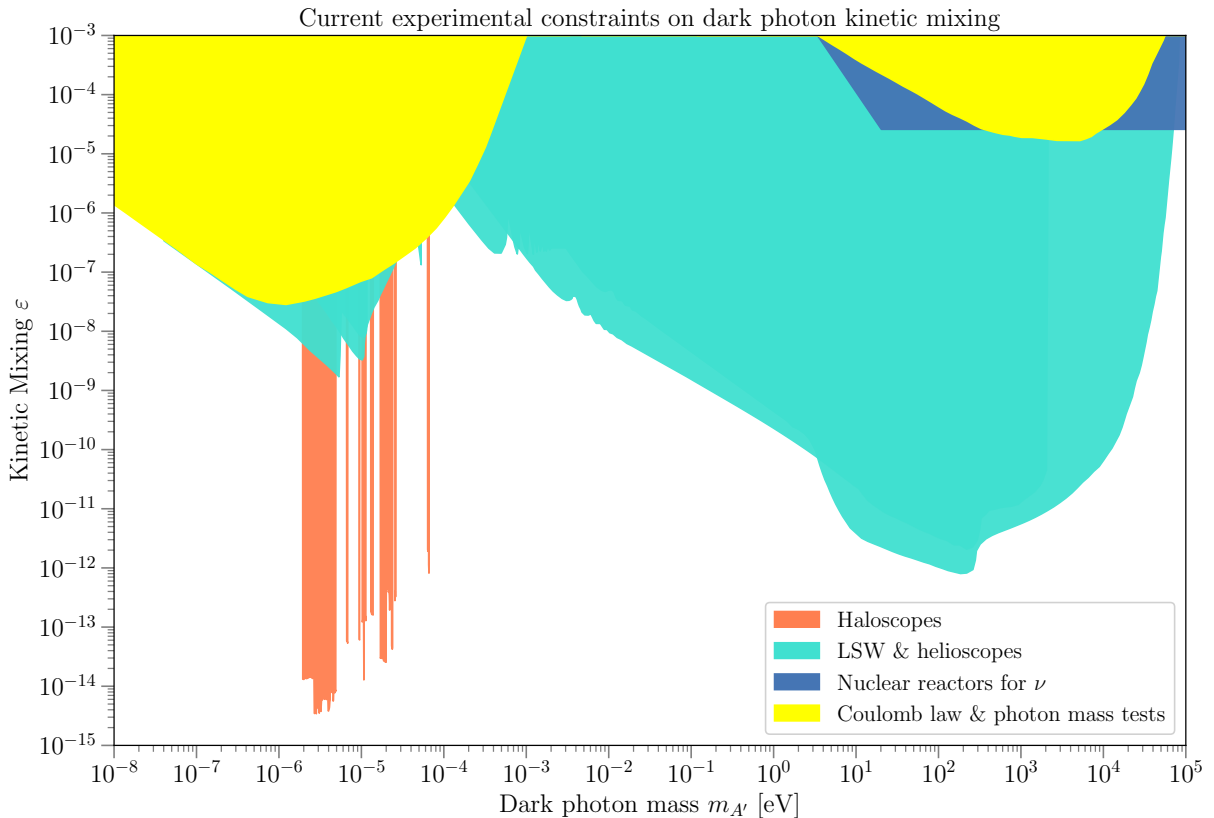


Figure 1. Upper exclusion limits in the parameter space of the dark photon mass $m_{A'}$ (x-axis) and the kinetic mixing parameter ϵ (y-axis). This figure shows only current experimental bounds, excluding those that assume the dark photon is a dark matter candidate, which is not considered in this work.

case of the dark photon, where the magnetic field is not necessary, as these particles can naturally mix with the SM photon. The probability of a dark photon converting into a photon depends on its mass and the length of the cavity [29].

These experiments provide an ideal framework for exploring BSM physics. The experimental constraints of both types of experiments can be directly applied to the case of massive dark photons. Among the main experiments of this type are: CAST [29], ALPS [30], CROWS [31], DARK SRF [32], HINODE [33], IAXO [34], LSW-AMDX [35], LSW-CERN [36], LSW-Spring-8 [37], LSW-UWA [38], and SHIPS [39]. These experiments continue to play a critical role in constraining the properties of dark photons and other BSM particles. The bounds from these experiments are presented in *turquoise* in Figure 1.

- *Nuclear Reactor Experiments:* Nuclear reactor-based experiments, such as GEMMA or TEXONO (Taiwan EXperiment On Neutrino), were originally designed to study

processes like $e^- \nu_{e^-} \rightarrow e^- \nu_{e^-}$. However, their results can also be interpreted in the context of photon-dark photon oscillations inside the reactor, much like the well-known neutrino oscillations. These experiments provide an additional avenue for studying dark photons due to the high intensity of electromagnetic fields present in nuclear reactors. The results published in [40] conclude that neutrino experiments are insensitive to dark photons with masses below ~ 0.1 eV. The bounds from Nuclear Reactors are presented in *blue* in Figure 1.

- *Haloscopes*: This experimental approach was first proposed in 1983 by Pierre Sikivie [41] as a technique to detect axions, a dark matter candidate. The method uses a resonant microwave cavity placed within a strong magnetic field. In this system, axions interact with the virtual photons generated by the magnetic field, producing an oscillating electromagnetic field whose frequency is proportional to the axion mass [28]. For this conversion to occur efficiently, the axion mass must fall within the range of frequencies that the microwave cavity can tune. Since the axion mass is unknown, the cavity’s resonance frequency must be continuously adjusted to explore a wide range of possible masses. The electromagnetic field generated inside the cavity is detected by a small antenna connected to an ultra-low-noise preamplifier. This system is designed to maximize the signal produced by axions while minimizing background noise, enabling a more efficient search across the mass parameter space. This approach emerged as an innovative solution for detecting axions, particles that cannot be observed using conventional methods based on accelerators or nuclear reactors due to their unique properties and well-defined mass range. Furthermore, the experimental limits established for axions can be adapted to set constraints on the dark photon. This is possible because, in theory, both axions and dark photons can oscillate into SM photons. This theoretical similarity allows the results of haloscope experiments to be extended beyond axions, providing new insights in the search for dark photons and other particles BSM. The bounds from Haloscopes are presented in *orange* in Figure 1.

- *Atomic and Coulomb law experiments*: The possible existence of a dark photon and its kinetic mixing parameter with ordinary photons could modify the Coulomb force at atomic distances, introducing an additional Yukawa-type potential,

$$V(r) = -\frac{Z\alpha}{r} (1 + e^{-m_{A'} r} \epsilon^2) ,$$

where $m_{A'}$ is the mass of dark photon and $\frac{Z\alpha}{r}$ is the usual Coulomb potential. The inclusion of this potential would perturb atomic energy levels, thereby enabling the indirect inference of a dark photon through high-precision spectroscopy. These modifications to the energy levels would alter the Rydberg limit established for the pure Coulomb case and would be observable in spectral transitions. Corrections to the Rydberg constant and the Lamb shift could experimentally translate into new limits on the parameter space of the dark photon, specifically its kinetic mixing term and

its mass [42, 43]. Key experiments designed to probe these effects include Plimpton-Lawton experiment, Cavendish-like experiments, AFM, Atomic Spectroscopy, among others [44]. The bounds from Atomic and Coulomb law experiments are presented in *yellow* in Figure 1.

In this work, however, we are interested in the photon-counting technique. Photon counting, as the name suggests, is a technique that involves counting individual photons using a photon counting detector (PCD). When a photon interacts with the detector’s material, it generates an electrical pulse whose amplitude is proportional to the photon’s energy. Among its main advantages, compared to traditional detectors, is the reduction of electronic noise, since measuring each photon individually results in a clearer signal. Additionally, this technique allows one to determine the energy of each photon through the use of energy thresholds. Some of the main detectors used in this method include photomultipliers, Geiger counters, and scintillation counters [45–47]. This technique is especially useful when dealing with processes with photons in the final state, being capable to measure low-energy photons.

4 The Dark Inverse Compton Scattering

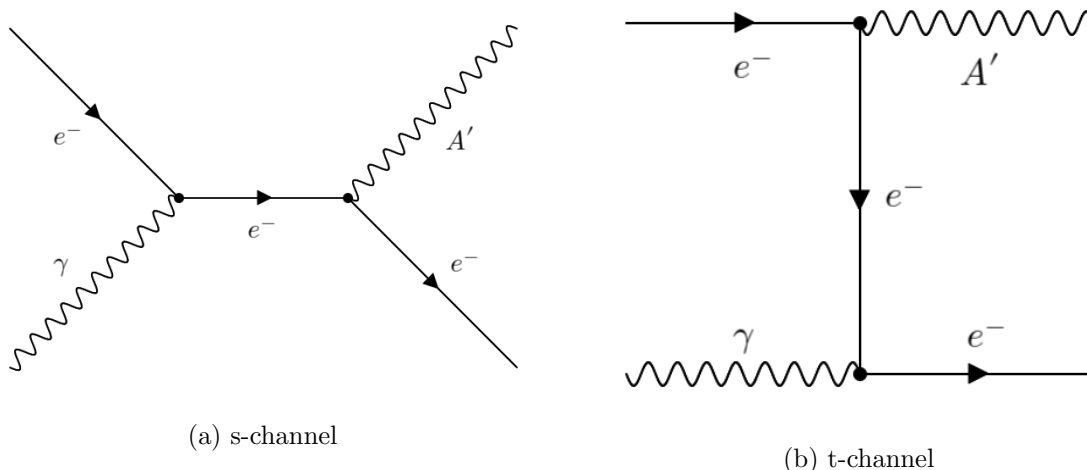


Figure 2. Feynman diagrams of the inverse Compton scattering production of dark photons.

The search for dark photons via the kinetic-mixing portal can be effectively pursued through the Dark Inverse Compton Scattering (DICS) process, $e^- \gamma \rightarrow e^- A'$. This mechanism, represented by the s - and t -channel Feynman diagrams in Figure 2, is analogous to standard inverse Compton scattering (ICS), with the key difference that the outgoing photon is replaced by a dark photon. The DICS cross section is proportional to the ICS one, scaled by the kinetic-mixing parameter squared, i.e. $\sigma_{\text{DICS}} \approx \varepsilon^2 \sigma_{\text{ICS}}$. The full expression, which depends on the dark-photon mass ($m_{A'}$) and the center-of-mass energy (\sqrt{s}), is given in Eq. (4.1). Despite the process being general to electron-photon collisions, the present analysis is inspired by the existing infrastructure at the Brazilian Synchrotron Light Laboratory

$$\begin{aligned}
\sigma = & \frac{g^2 g'^2}{8\pi(s - m_e^2)^3} \left[\frac{s^3 + 15m_e^2 s^2 - m_e^4 s + m_{A'}^2 (7s^2 + 2m_e^2 s - m_e^4) + m_e^6}{2s^2} \right. \\
& \times \sqrt{(s - m_e^2)^2 - 2m_{A'}^2 (s + m_e^2) + m_{A'}^4} + (s^2 - 6m_e^2 s - 2m_{A'}^2 (s - m_e^2) - 3m_e^4 + 2m_{A'}^4) \\
& \left. \times \log \left(\frac{s + m_e^2 - m_{A'}^2 + \sqrt{(s - m_e^2)^2 - 2m_{A'}^2 (s + m_e^2) + m_{A'}^4}}{s + m_e^2 - m_{A'}^2 - \sqrt{(s - m_e^2)^2 - 2m_{A'}^2 (s + m_e^2) + m_{A'}^4}} \right) \right].
\end{aligned} \tag{4.1}$$

(LNLS), which hosts an electron accelerator named SIRIUS. This is needed because the experimental setup and new physics reach heavily rely on the technical details of the accelerator setup. The cross-section behavior as a function of $m_{A'}$ (Figure 3), evaluated for

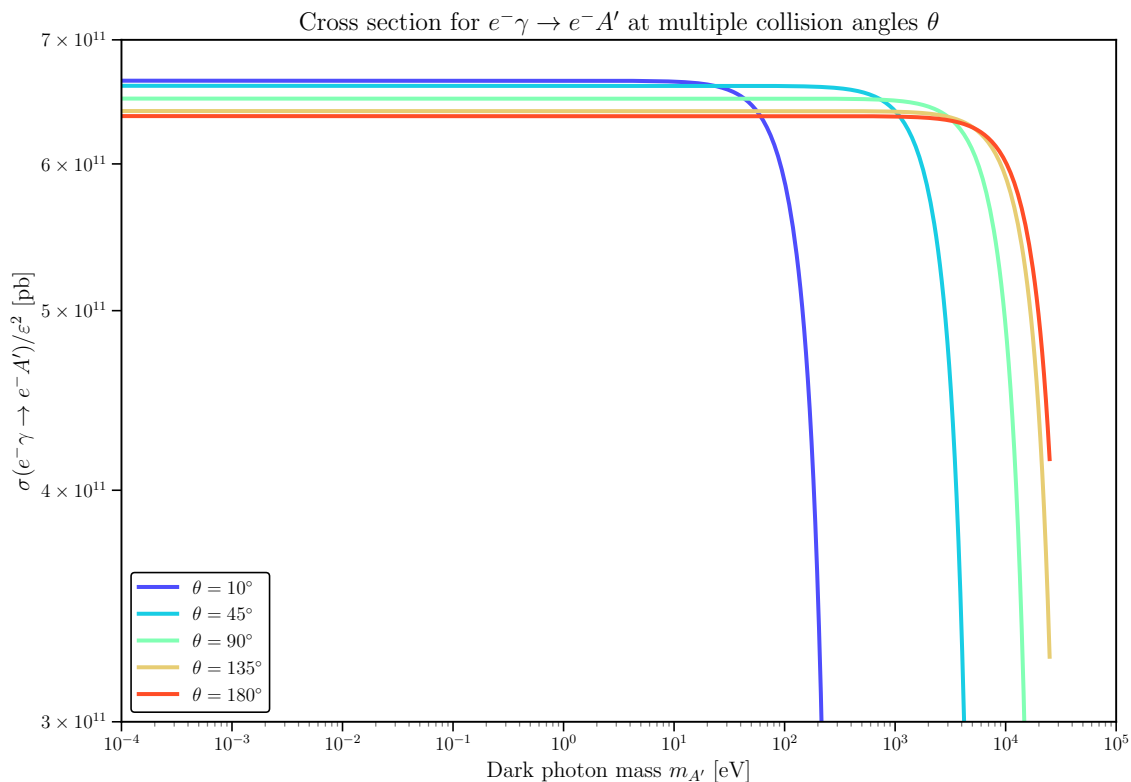


Figure 3. Cross section for $e^- \gamma \rightarrow e^- A'$ as a function of the dark photon mass $m_{A'}$ for different collision angles θ . The plotted cross section is normalized by ε^2 , allowing the results to be rescaled for any choice of the kinetic mixing parameter ε .

various collision angles θ , shows that the ideal head-on configuration ($\theta = 180^\circ$) maximizes sensitivity to higher dark-photon masses due to the angular dependence of \sqrt{s} . Differences between $\theta = 135^\circ$ and $\theta = 180^\circ$ are minimal, which justifies the near-head-on approxi-

mation adopted in our projections and enables sensitivity to masses up to $\sim 3 \times 10^4$ eV. At very small angles ($\theta < 10^\circ$), the cross section develops infrared divergences that are rendered irrelevant by the experimental energy thresholds.

For numerical estimates, we employ the parameters of the Sirius accelerator: an electron-beam energy of 3 GeV and a laser-photon energy of 1 eV ($\lambda = 1240$ nm). The dependence of the cross section on the laser wavelength (Figure 4), shown here for $m_{A'} = 1$ keV, indicates an optimal sensitivity band for λ between 400 nm and 4000 nm. The chosen 1 eV laser lies well within this region, particularly for $\theta \geq 135^\circ$. For more oblique collisions ($\theta < 45^\circ$), shorter-wavelength lasers would be advantageous to compensate for the reduced phase space.

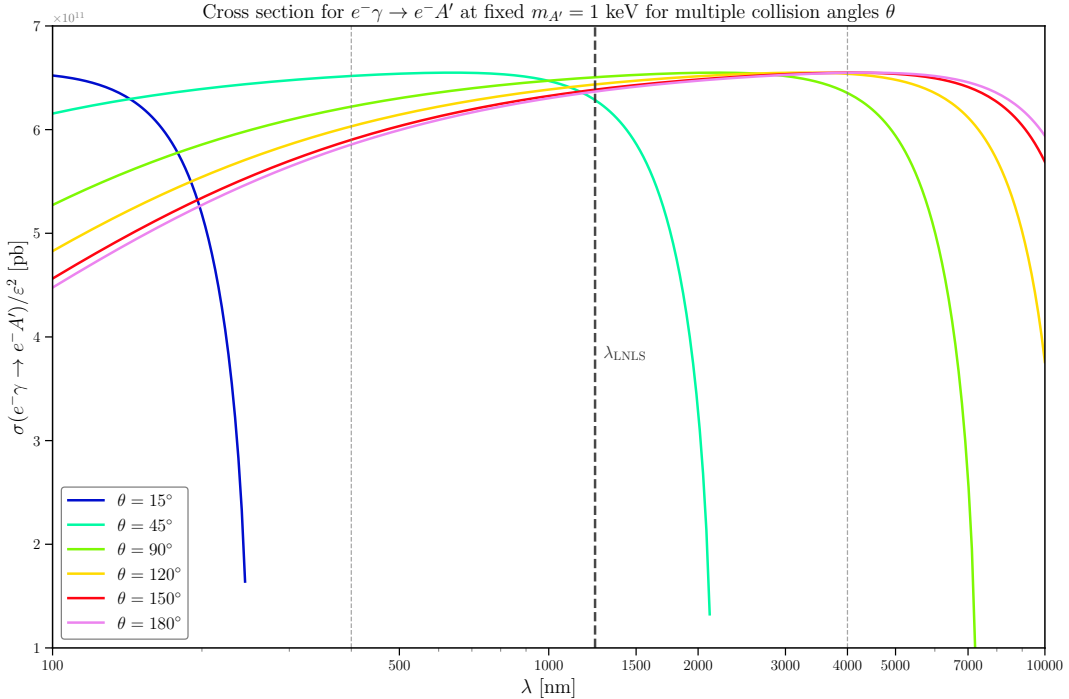


Figure 4. Cross section $\sigma(e^- \gamma \rightarrow e^- A')$ normalized by ε^2 as a function of the laser wavelength λ for different collision angles θ , with fixed dark photon mass $m_{A'} = 1$ keV. The vertical gray dashed lines indicate the optimal sensitivity region, $400 \text{ nm} \leq \lambda \leq 4000 \text{ nm}$, and the black dashed line shows the wavelength used in this work ($\lambda \simeq 1 \text{ eV}$), corresponding to a 1 eV laser beam. This figure is shown for illustrative purposes to highlight the variation of the cross section with wavelength and incidence angle.

Since the dark photon is expected to be invisible in the sub-MeV mass range considered here, detection must rely on indirect methods. We propose two complementary techniques: (i) photon counting, performed with an Avalanche Photodiode (APD) capable of detecting deficits in the expected Compton-scattered photon yield, and (ii) missing-energy measurements in the scattered-electron spectrum, using a high-resolution spectrometer. The feasibility of the latter requires achieving an energy resolution $\Delta E/E \lesssim 10^{-4}$, a value attainable with modern calorimetric systems. The following section details the implementation of this

experimental strategy.

5 Experimental Setup

This work presents a preliminary sensitivity study and a proposal for searching for low mass dark photons. As aforementioned, this study could be generalized to different electron accelerators that could be operated to conduct electron-photon collisions. However, the proposal of an experimental setup demands more technical details, and for this reason, we will target our analysis to the existing electron accelerator at Sirius [17]. The facility accelerates electrons to 3 GeV and provides high-brilliance synchrotron radiation, which is used in many fields of science, such as biology, chemistry and others. Our focus, however, is on the electron beam, which can be used to investigate BSM physics. Particularly, we propose to search for a dark photon A' , which may belong to the hidden sector of the universe. The proposed experimental setup, which enables searches for new particle

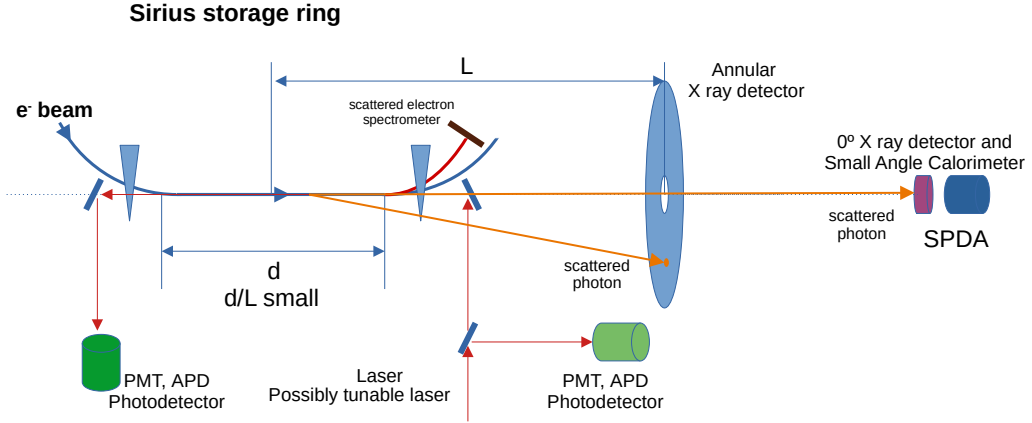


Figure 5. Proposed experimental setup of the experiment illustrating an electron beam (green) with an energy of 3 GeV colliding with a laser of $\mathcal{O}(\text{eV})$ positioned at a certain angle to produce dark photons. The X-ray detectors (and/or calorimeters for high energy photons) detect predominantly background photons.

production in the process $e^- \gamma \rightarrow e^- A'$ is shown in Figure 5. It employs an $E_e = 3$ GeV electron beam from the Sirius facility that will collide with a $E_\gamma \sim \mathcal{O}(1 \text{ eV})$ monochromatic laser, operating at a pulse frequency of 100 MHz and emitting $\sim 10^{16}$ photons per pulse. Sirius electron beam has a nominal current of 350 mA [48], ensuring $\sim 2 \times 10^{18}$ particles per second to serve as back-scattering targets for Compton-like process through interactions of the form $e^- \gamma \rightarrow e^- A'$. The laser is placed within a cavity measuring 10^{-6} m on both the x and y axes, similar to the transverse dimensions of the electron beam. The total available center of mass energy is sufficient for the production of particles with mass up to

$m_X \simeq \frac{2E_\gamma E_e}{m_e} \simeq \mathcal{O}(10 \text{ keV})$, together with a scattered electron. This limits the sensitivity to low-mass dark photon and/or axion like particles search. Since the total available transverse energy is $\leq \mathcal{O}(10 \text{ keV})$, the beam electron which served as a scattering target continues to move predominantly in the forward direction together with the rest of the beam particles until the first dipole magnet along the storage ring. Due to its reduced momentum after scattering, it experiences a larger magnetic deflection, enabling its separation from the primary beam envelope. The scattered photons include a high-energy component emitted predominantly forward along the electron beam, and a lower-energy component at larger angles. This motivates the placement of both forward and large-angle photon detectors.

Since A' , even if produced in the $e^- \gamma$ scattering, will remain undetected due to the suppressed by ε interaction cross-section, the possible experimental signature is limited only to several possible observables:

- Registration of potential change in the total flux of the Compton scattered photons with respect to the expected number of photons, as calculated within QED and simulated with MC methods, as a function of the laser photon energy and incident angle.
- Modification of the spectrum of the Compton scattered photons within a given region in the $(\theta_\gamma, E'_\gamma)$ parameter space, due to the existence of a competing interaction process, which effectively (and indirectly) appears as a change in the $\frac{d\sigma}{d\theta_\gamma dE'_\gamma}$.
- Appearance of a low-energy electron with no higher energy accompanying photon (i.e. missing energy).

The first two observables are related to the search of a small change in the expected number of particles, which is proportional to ε^2 . The change could be detected by precise flux measurements in the scattered or non-interacted beam, which requires accurate flux normalization and long-term stability of the laser and electron beam conditions.

Photon detection is achieved through two complementary systems: first, an annular ring calorimeter, exposed predominantly to photons with energy in the $\mathcal{O}(10 - 100 \text{ keV})$ up to 1 MeV range, to measure the energy spectrum of photons at large angles, and second, single-photon detection array (SPDA) for time-resolved photon counting, coupled to a laser monitoring system.

The SPDA serves as the primary sensor for missing-energy detection. It can be implemented as a multi-section array, with each section optimized to detect a specific energy range of the recoil photon spectrum, ensuring full coverage from low to high energy photons. By providing time-resolved single-photon counting synchronized with the laser pulses, the SPDA enables precise identification of photon deficits corresponding to potential dark photon production. The section devoted to optical photons registration could be realized as a semiconductor device (e.g. array of low-noise high-gain single photon avalanche diodes (SPADs) [49], e.g. silicon photomultipliers (SiPMs) [50]). When operated under reverse voltage above the breakdown threshold, this semiconductor device converts individual photons into measurable electrical signals through avalanche multiplication. This process exploits the photoelectric effect to amplify faint signals, enabling single-photon

detection with nanosecond timing resolution. Alternatively, multi-anode conventional photomultipliers could also be employed for direct optical photon detection at the expense of a larger material budget and possible absorption of part of the X-ray photons. The X-ray section could be made of a high-density, high- Z semiconductor material like Cadmium Telluride (CdTe) or Cadmium Zinc Telluride (CZT), attached to a photodetector, or a high-efficiency inorganic scintillator like CsI(Tl) [51]. These materials offer superior absorption efficiency for X-rays compared to plastics, due to their higher atomic number (Z) and density [52]. However, plastic scintillators based on bulk polymerization feature high light yield and uniformity and have the advantage of fast emission which could allow better double pulse separation and high rate capabilities. The higher photon energy section could be made as a conventional crystal electromagnetic calorimeter detecting photons in the $\mathcal{O}(10 \text{ MeV}) - 1 \text{ GeV}$ range. Inorganic scintillators such as BGO ($\text{Bi}_4\text{Ge}_3\text{O}_{12}$), LSO, LaBr_3 and CeBr_3 are appropriate for $\mathcal{O}(\text{MeV})$ photon energy due to their high light yield and high Z value, which enhances detection efficiency for Gamma-rays [53], while for $E_\gamma > 50 \text{ MeV}$ Cherenkov light crystals like PbF_2 are the proper choice, allowing single gamma counting with sub-ns time resolution and pulse duration [54, 55].

By comparing the expected photon flux (calculated from laser intensity and Compton cross-sections) with the SPDA measured counts, statistically significant deficits would indicate missing energy from non-interacting dark photons. The calorimeter simultaneously records the photon energy distribution, allowing cross-verification of spectral anomalies.

The photons with larger energy will be accompanied by higher energy loss of the corresponding target electron. Thus the recoil electron will possess lower energy than the nominal Sirius beam energy and will be deflected stronger by the first dipole magnet after the Compton scattering region, allowing its detection with a segmented charged particle detector. Silicon pixel detectors with high resolution, e.g. Timepix3-based arrays [56, 57] or monolith active pixel sensors [58–60] could provide charged particle detection with $\mathcal{O}(\text{ns})$ time resolution and $50 \mu\text{m}$ pixel size. The smaller the pixel size, the better the e^- resolution would be. Event identification can be performed by matching the electron momentum with the photon energy in the annular calorimeter (less probable) or the small angle calorimeter. This configuration enables searches for new particle production when the invariant mass of the final state approaches $m_e + m_{A'}$ through event-by-event missing energy search.

The proposed setup also features a set of laser control detectors (APD, PMT or other), allowing to precisely follow the laser beam intensity and to measure the flux of the non-interacted laser photons. This monitoring system will operate continuously, providing flux normalization and tracking pulse-to-pulse variations. It can also serve as an independent detector to probe potential disappearance of laser photons in undetected final-state channels. This multi-detector approach provides robust information which could constraint the dark photon mass $m_{A'}$ and coupling parameter ε , with particular sensitivity to feeble interactions. The combined scattered photon detection system exploits the APD’s single-photon counting capability, when operated in Geiger mode, and the calorimeter’s energy resolution to isolate potential dark photon signatures from instrumental effects. To fully exploit this capability, the experiment must ensure sensitivity to photon energies extending into the near-infrared and sub-eV regime.

The optical photon detection system is designed to provide broad spectral coverage, ensuring sensitivity to potential photon disappearance events. In addition to SPAD/APD-based sensors and SiPM arrays optimized for visible wavelengths, near-infrared photomultiplier (NIR-PMT) modules may be incorporated to extend efficient single-photon detection down to photon energies of approximately 0.7 eV. These devices offer lower dark count rates and improved quantum efficiency in the NIR compared to room-temperature semiconductor photodiodes, requiring only moderate cooling (e.g., liquid-nitrogen temperatures). Together with the semiconductor photon counters, they establish the effective low-energy detection threshold of the optical system. Sensitivities below this range require cryogenic detector technologies, whose implementation and performance considerations are discussed in Section 6. This layered approach ensures continuous coverage from optical to sub-eV photon energies and defines the thermal and cryogenic requirements of the overall detection strategy. This extended spectral coverage is essential for identifying potential missing-energy signatures associated with dark photon production.

In particular, the presence of missing energy signature in the analysis of photon energy distributions or in the single events with detected lower energy electron could provide critical constraints on the mass and coupling constant of the dark photon, thereby enhancing our understanding of dark matter candidates and the hidden sector of the universe. This method builds upon established missing-energy techniques used in supersymmetry and dark matter searches [61–63], but adapts them to the unique capabilities of synchrotron light sources. The results from this experiment could significantly advance our knowledge of the DP parameter space and their potential role as mediators between the SM and dark matter.

6 Lower Photon Detection Thresholds

To enable the detection of photon disappearance events indicative of dark photon production, the key technological challenge is to achieve high-efficiency photon counting at low energies, particularly in the near-infrared (NIR), mid-infrared (MIR), and extending into the terahertz (THz) spectral range. This requires cryogenic operation and a careful selection of detector architectures optimized for different parts of the energy spectrum.

As discussed in the experimental setup, the optical detection system establishes the effective low-energy threshold of the experiment. In the initial stage, for photon energies down to approximately 0.7 eV (corresponding to wavelengths up to $\approx 1.7 \mu\text{m}$), we propose the use of a near-infrared photomultiplier module. Such devices provide efficient single-photon detection above this threshold with moderate cooling (e.g., liquid-nitrogen temperatures) and complement semiconductor photon counters used at visible wavelengths. This provides a robust and commercially available platform for performing initial absence measurements. Below this energy range, the quantum efficiency of photomultiplier tubes rapidly decreases near the long-wavelength cutoff, making superconducting cryogenic detectors necessary to extend the sensitivity toward lower photon energies.

For the 0.1–0.7 eV range, Superconducting Nanowire Single-Photon Detectors (SNSPDs) present a highly promising option. SNSPDs based on materials such as tungsten silicide

(WSi) or molybdenum silicide (MoSi) exhibit excellent quantum efficiency in the NIR and MIR range, with detection efficiencies up to 90% and dark count rates below 1 count per second when cooled to sub-Kelvin temperatures. Their fast response times (< 100 ps) make them well-suited for time-resolved photon counting. Although standard SNSPDs become inefficient below ~ 0.1 eV, ongoing developments in material engineering and antenna-coupled geometries are progressively pushing this limit toward lower energies.

For the $0.01 - 0.1$ eV regime, corresponding to far-infrared and THz photons, two alternative technologies are under consideration: Kinetic Inductance Detectors (KIDs) and Superconducting Tunnel Junctions (STJs). KIDs are intrinsically multiplexable, cryogenic detectors that can be engineered for broadband absorption and are particularly effective for THz photon detection. Their typical energy thresholds extend down to a few meV, making them ideal for waveguide- or antenna-coupled setups in a dilution refrigerator. While their time resolution ($\sim \mu\text{s}$) is lower than that of SNSPDs, their scalability and low noise performance make them well-suited for large-area, background-limited measurements.

STJs offer a complementary approach, providing intrinsic energy resolution and single-photon sensitivity down to photon energies of \sim meV. Their operation relies on detecting quasiparticles generated by photon absorption in a superconducting junction, yielding energy-resolved spectra that can help discriminate signal from background. However, they suffer from longer integration times and more complex readout electronics, making them more suitable for targeted energy-tagging applications rather than high-rate detection.

Together, these technologies can be integrated into a tiered detection strategy that covers the sub-eV energy range down to the meV scale. In such a configuration, SNSPDs would handle higher-energy (NIR-MIR) photons, while KIDs and STJs would cover the lower-energy THz regime. Note that while the NIR measurements can be performed off axis, for the even lower detection energies waveguides can be efficiently used to inject the photons into the cryogenic setup that will be a larger piece of equipment than the NIT-PMT setup. This multimodal approach, will use cutting edge cryogenic quantum technology, and ensure maximal sensitivity across the desired spectrum and enables robust identification of photon disappearance events as signatures of new physics.

The motivation for extending the photon detection threshold toward the sub-eV range is directly connected to the angular structure of inverse Compton scattering shown in Fig. 6. In the laboratory frame, the emitted photons are strongly forward-collimated, with the highest energies concentrated inside the relativistic cone of opening angle $\sim 1/\gamma$. Away from this cone, the scattered-photon energy decreases rapidly, producing a broad population of lower-energy photons at larger angles. Consequently, increasing the angular acceptance of the detector alone does not significantly enhance the measurable photon flux unless the detector remains efficient at low energies.

Lowering the detection threshold therefore enlarges the experimentally accessible phase space in two coupled ways: it enables detection of soft photons emitted at large angles, and it allows wider angular coverage to contribute meaningfully to the total photon statistics. In practice, however, the angular acceptance used in the analysis is optimized through cuts, since very large angles are dominated by soft-photon backgrounds that do not improve sensitivity to missing-energy signatures. The extended energy-angle coverage thus improves

photon-counting and flux-deficit measurements by increasing the number of detected Standard Model ICS photons used for normalization, while timing, geometric, and kinematic selections suppress the additional background associated with the enhanced soft-photon flux.

7 Discussion

7.1 Background

The main background arises from the SM photons generated in the inverse Compton scattering process. These photons exhibit a well-defined energy and angular distribution, peaking at forward angles with energies up to ~ 132 MeV [64]. Since we'll use a photon counting approach, it's necessary to know the number of photons produced by the SM ICS when assuming the experiment's configuration in order to have a reliable estimative of the background. To generate this background, we calculated the angular distribution of the number of photons per bin, presented in Figure 6, assuming the scenarios of 3 months and 1 year of data. As the experiment is expected to produce a high number of photons, we can use this result to develop a strategy in order to reduce the background and make sure that the equipment is capable of reliably detect these photons. The behavior of the curves points to the fact that the number of background events can be reduced by applying kinematic cuts in the analysis for scattering angles $135^\circ \leq \phi \leq 180^\circ$ and $0^\circ \leq \phi \leq 45^\circ$, corresponding respectively to backscattering and forward scattering regions. This feature is enhanced with a longer period of data acquisition, as expected. The deviations from this prediction either in energy or in photon count, serve as signatures of dark photon production. For further details on the angular distribution of the dark photon flux, see Appendix B.

7.2 Projected Sensitivity

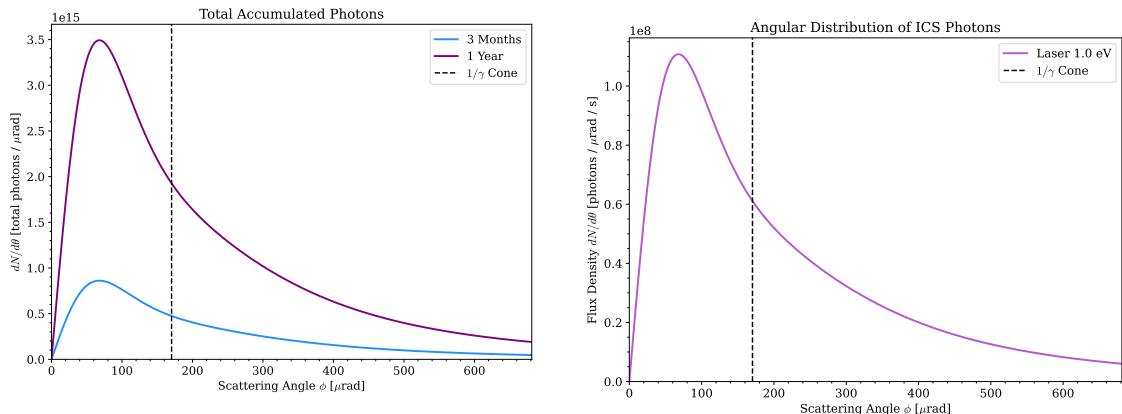
The projected bounds on the dark photon kinetic mixing parameter as a function of its mass, shown in Figure 7, were derived using the standard significance estimator

$$\text{Significance} = \frac{N_s}{\sqrt{N_s + N_b}} \simeq \frac{\sigma_s}{\sqrt{\sigma_s + \sigma_b}} \sqrt{\mathcal{L}_{\text{int}}}, \quad (7.1)$$

where N_s and N_b denote the expected number of signal and background events, respectively, and \mathcal{L}_{int} is the total integrated luminosity. The background contribution N_b is evaluated including the expected SM background from ICS photons under realistic beam conditions. Incorporating the angular cuts described in Section 7.1 reduces N_b by excluding photons in regions of low signal expectation, improving the overall significance.

The integrated luminosity for one year of data taking is obtained by multiplying the instantaneous luminosity,

$$\mathcal{L}_{\text{inst}} = \frac{N_1 N_2 f N_{\text{bun}}}{2\pi \sqrt{\sigma_{1x}^2 + \sigma_{2x}^2} \sqrt{\sigma_{1y}^2 + \sigma_{2y}^2}}, \quad (7.2)$$



(a) Total of photons accumulated in 1 year and 3 months

(b) Total of photons per second

Figure 6. Angular distribution of the number of photons per bin for the SM ICS background. The left panel (a) shows the total accumulated photons for scenarios of 3 months and 1 year of data acquisition, while the right panel (b) displays the total number of photons produced per second. As can be seen, the majority of the produced photons are highly collimated, situated within the relativistic cone defined by $1/\gamma$.

by the total running time of one year, t_{year} :

$$\mathcal{L}_{\text{int}} = \mathcal{L}_{\text{inst}} \cdot t_{\text{year}}. \quad (7.3)$$

Here, N_1 and N_2 are the number of particles per bunch, f is the collision frequency, N_{bun} the number of bunches, and σ_{ix}, σ_{iy} the transverse beam dimensions. Using the nominal parameters of the Sirius accelerator and a 1 eV laser, this yields an integrated luminosity of $\mathcal{L}_{\text{int}} \approx 2.41 \times 10^{10} \text{ pb}^{-1}$ for one year of operation.

The projections reveal that Sirius can probe an unexplored parameter space in the range $10^{-8} \lesssim \varepsilon \lesssim 10^{-6}$, particularly for $m_{A'} \lesssim 10^4 \text{ eV}$. This complements existing constraints from astrophysical observations and other laboratory experiments, as shown in Figure 1. In the case of an oblique collision ($\theta < 180^\circ$), the analytic expression for the amplitude $\mathcal{M}(e^- \gamma \rightarrow e^- A')$ has been derived in [13] for the case of an incident polarized photon beam. The cross section peaks at $\theta = 180^\circ$; nevertheless, for $150^\circ \leq \theta \leq 180^\circ$, variations in its values are minor in most of the parameter space. The analysis of the variation of the cross section (Eq. (4.1)) with the wavelength of the laser is shown in Figure 4. So, the best-case scenario would be a near head-on collision, allowing the production of heavier dark photons. We remind the reader that this theoretical proposal aims to show the capabilities to constrain dark photon masses and mixings in a future dark sector detector, so we focus on the most ideal setup ($\theta = 180^\circ$) for calculating these projected bounds. For more details on the electron energy distribution relevant to these projections, see Appendix A.

Although our reasoning has been based on the coupling of dark photons with SM photons, the experimental strategy can obviously be applied to search for axion-like particles (ALPs) coupled to electrons, as well as other feebly interacting light scalars. Naturally, the production cross-section of those particles is different. Thus, an entirely new analysis

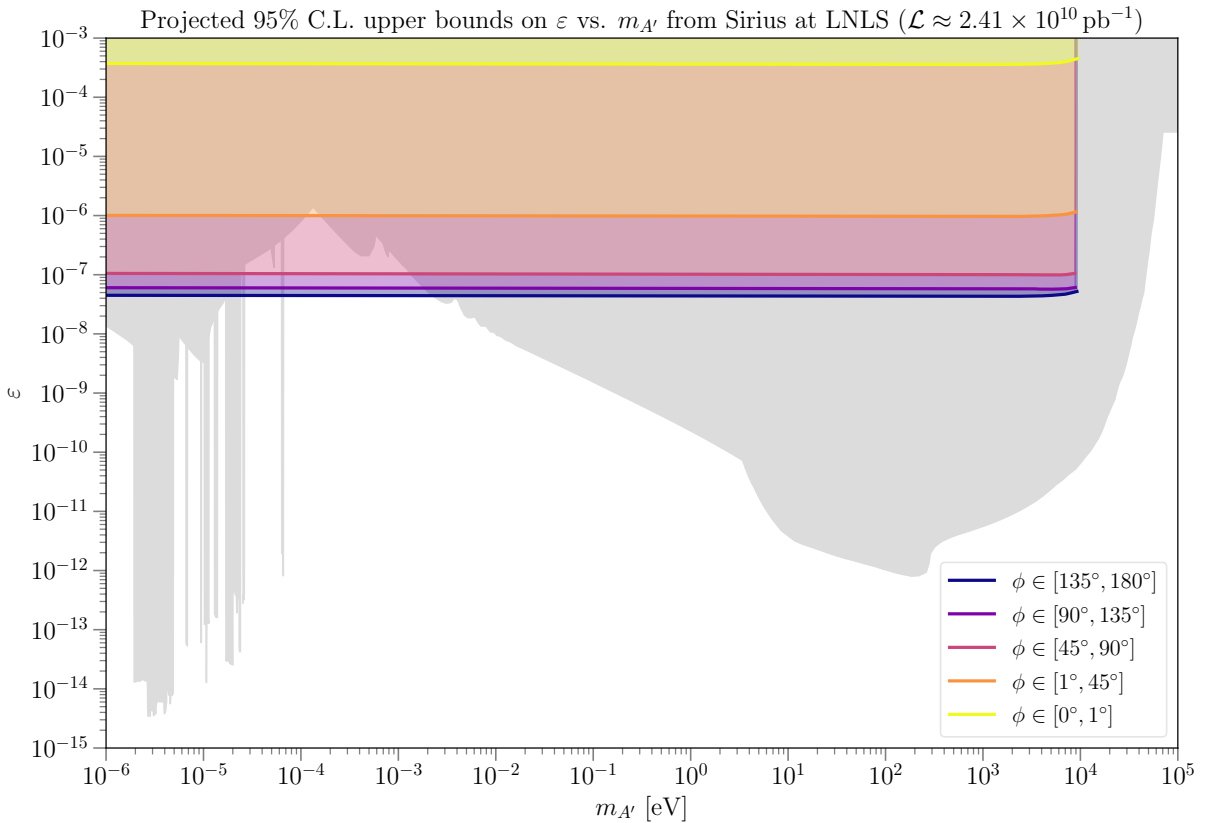


Figure 7. Projected 95% C.L. upper bounds (corresponding to a 2σ criterion as a proxy) on the dark photon kinetic mixing ε as a function of its mass $m_{A'}$, from Sirius at LNLS with $E_{e^-} = 3$ GeV and $E_\gamma = 1$ eV. Colored bands correspond to different kinematic cuts in the scattering angle ϕ for 864 bunches. Each band shows the upper bound region for its respective cut, extending continuously upward, with colors adjusted to avoid overlap. The bands represent 1-year sensitivities assuming an integrated luminosity of $\mathcal{L} \approx 2.41 \times 10^{10} \text{ pb}^{-1}$ obtained from Eq. (7.3), including a realistic background from inverse Compton scattering (ICS) photons.

would have to be performed. We leave this for future work. Nevertheless, it is important to stress that our work can serve as a platform to probe light particles with masses in the sub-eV range and below using accelerators in an orthogonal way to existing proposals [65–72].

8 Conclusions

In this work, we have proposed a novel experimental setup for the production and indirect detection of dark photons via inverse Compton scattering. For concreteness, we adopted the detector parameters existing at the Sirius accelerator. By exploiting the high-intensity 3 GeV electron beam and combining it with a 1 eV monochromatic laser, we explored the production channel $e^- \gamma \rightarrow e^- A'$, where A' denotes an invisible dark photon. The associated cross section, given in Eq. (4.1), exhibits a strong dependence on the dark

photon mass $m_{A'}$ and the collision angle θ , with optimal sensitivity for head-on collisions ($\theta = 180^\circ$), although configurations with $\theta \geq 135^\circ$ remain feasible.

We have computed the cross section for different collision angles and laser wavelengths, as shown in Figure 3 and Figure 4, establishing the ideal operating conditions for dark photon masses below $\mathcal{O}(10^5)$ eV. The variation with laser wavelength indicates that a 1 eV laser (corresponding to $\lambda = 1240$ nm) lies within the optimal range for probing the targeted mass window.

The projected bounds on the kinetic mixing parameter were derived for an integrated luminosity of $\sim 2 \times 10^{10}$ pb $^{-1}$, taking into account realistic parameters for the bunch structure and beam profile. The sensitivity curves presented in Figure 7 illustrate that, even assuming conservative background conditions, the proposed setup is capable of probing kinetic mixing values down to $\varepsilon \sim 10^{-8}$ for $m_{A'} \lesssim 1$ MeV, covering an unexplored region of parameter space.

Given that dark photons in this mass range do not decay into visible final states, their detection relies on indirect techniques. We have proposed a dual approach: *photon counting* and the *missing energy technique*. The first strategy searches for statistical deficits in the photon flux expected from standard inverse Compton scattering, detectable with devices such as avalanche photodiodes (APDs) or conventional photomultiplier tubes (PMTs). The second infers the presence of A' through an energy imbalance in the final-state electron, measurable with a high-resolution spectrometer. Both strategies require excellent control of systematic uncertainties and precise energy resolution, particularly to differentiate signal from background processes such as beamstrahlung or Compton backscattering.

The experimental setup can also be implemented to search for axion-like particles coupled to electrons. In this case, interactions of the form $e^- + \gamma \rightarrow e^- + a$ would produce similar missing energy signatures in the scattered electron and photon spectra. By employing precise photon counting and high-resolution electron spectrometry, the same setup proposed for dark photon searches could establish competitive bounds on the axion-electron coupling g_{ae} , opening an additional avenue for dark sector searches.

Overall, the proposed experiment presents a competitive and complementary approach to existing astrophysical and fixed-target searches. It serves as a platform to search for light particles in accelerators in the sub-eV mass range and below, with the potential to probe currently inaccessible regions of parameter space.

A Energy distribution of the electron in DICS process

The energy spectrum of the outgoing electron in the process $e^- \gamma \rightarrow e^- A'$ is shown in Fig. 8. As can be seen, there is a large fraction of events where the electron misses $\mathcal{O}(100 \text{ MeV})$ energy, and the presence of a photon with such energy should be detectable with inefficiency less than 10^{-4} .

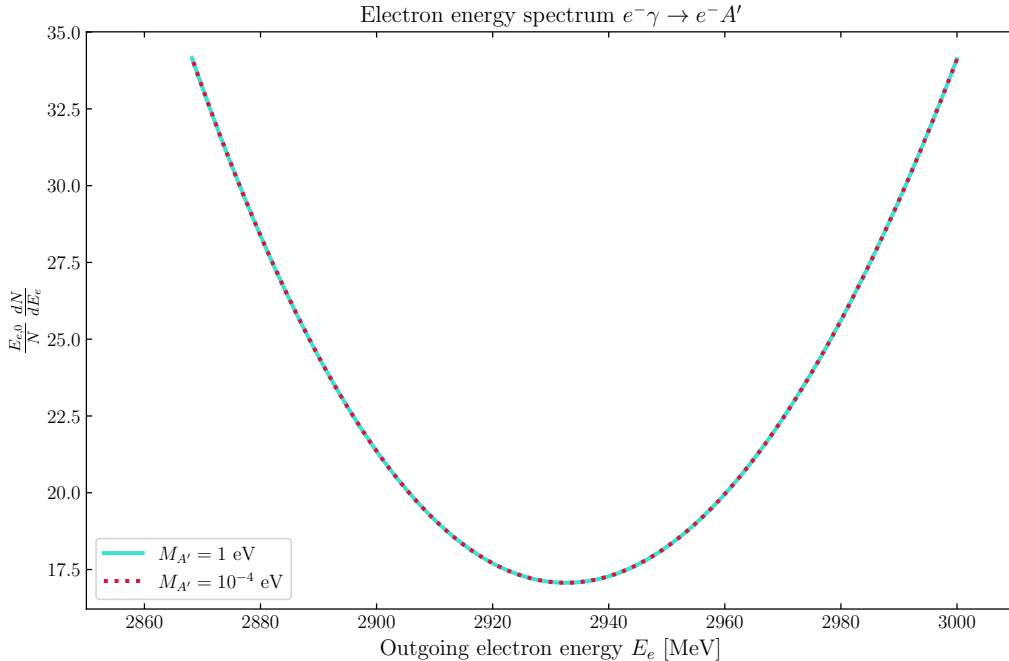


Figure 8. Normalized energy spectrum of the outgoing electron in the process $e^- \gamma \rightarrow e^- A'$ for two values of the dark photon mass, $M_{A'} = 1 \text{ eV}$ (solid turquoise) and $M_{A'} = 10^{-4} \text{ eV}$, and kinetic mixing $\varepsilon = 10^{-7}$. The spectra are normalized such that $\int dE_e (E_{e,0}/N) dN/dE_e = 1$. Differences between the two masses are negligible due to the ultralight nature of the dark photon relative to the beam energy ($E_{e,0} = 3 \text{ GeV}$).

B Flux of Dark Photons as a Function of the Scattering Angle ϕ

In this appendix, we illustrate the flux of dark photons as a function of the scattering angle ϕ , considering a dark photon mass of $M_{A'} = 1 \text{ eV}$ and a kinetic mixing parameter $\varepsilon = 10^{-7}$.

The Figures 9 and 10 are particularly important because they provide crucial information for designing the experimental geometry and optimizing the detection strategy. The experiment aims to produce dark photons and infer their existence through two techniques: direct detection of photons and electrons in the final state, and indirect detection via SM photon counting and missing energy. In this context, SM photons act as background, while the signal corresponds to the missing energy in the reconstructed final state, which could be carried away by dark photons. By analyzing the angular distribution of the dark photon

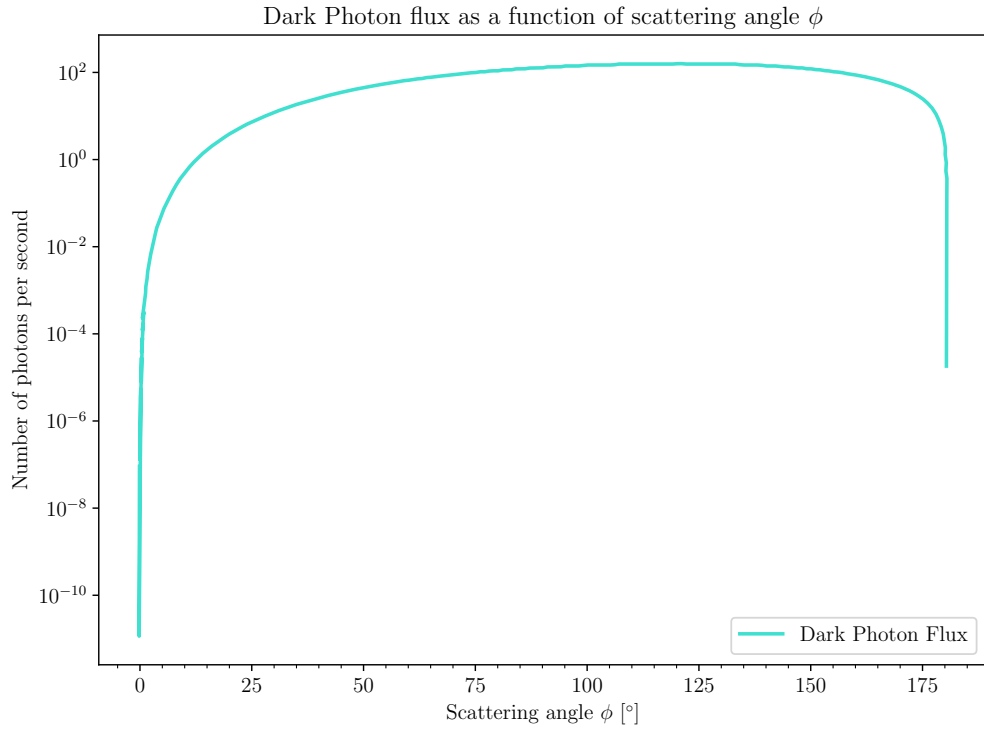


Figure 9. Flux of dark photons per second as a function of the scattering angle ϕ for $M_{A'} = 1$ eV and $\varepsilon = 10^{-7}$.

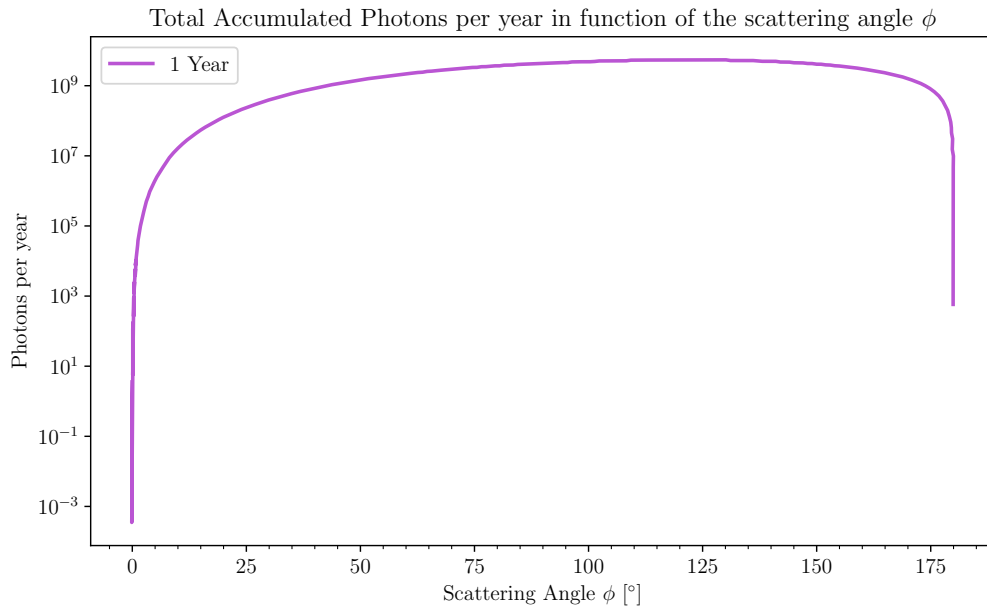


Figure 10. Flux of dark photons per year as a function of the scattering angle ϕ for $M_{A'} = 1$ eV and $\varepsilon = 10^{-7}$.

flux, we can identify the regions of the detector with the highest expected signal and plan the sensor placement accordingly.

Acknowledgments

The authors thank Harry Westfahl from the Sirius accelerator for providing useful information about the accelerator, which is essential to developing this work. We also appreciate the discussions with Bertrand Laforge, Paolo Crivelli, Felix Kahlhoefer, Manfred Lindner and Seokhoon Yun to improve this proposal. FSQ is supported by Simons Foundation (Award Number: 1023171-RC), Humboldt Foundation, and ANID - Millennium Science Initiative Program - ICN2019_044., IIF-FINEP grant 213/2024, FAPESP Grants 2021/14335-0 and 2021/00449-4, CNPq grants 307130/2021-5, 403521/2024-6, 309465/2026-5, and 446711/2025-0. LA acknowledges support from the Coordenação de Aperfeiçoamento de Pessoal de Nível Superior (CAPES) under grants 88887.827404/2023-00 and 88881.128190/2025-01. LA also thanks the Department of Physics at the University of Oslo for support and useful discussions during the final stage of this work. GG acknowledges support from Universidad Nacional de Ingeniería funding Grant FC-PFR-26-2025. V.K. recognizes support by project SUMMIT BG-RRP-2.004-0008-C01 and by BNSF KP-06-COST/25 from 16.12.2024 based upon work from COST Action COSMIC WISPerS CA21106 supported by COST (European Cooperation in Science and Technology). ASJ acknowledges support from FAPESP under the grant 2023/13126-4. JS acknowledges support from the UK Research and Innovation Future Leader Fellowship MR/Y018656/1. We also thank IIP for the local cluster *bulletcluster*, which was instrumental in this work.

References

- [1] H. Andernach and F. Zwicky, *English and spanish translation of zwicky's (1933) the redshift of extragalactic nebulae*, [1711.01693](#).
- [2] V.C. Rubin and J. Ford, W. Kent, *Rotation of the Andromeda Nebula from a Spectroscopic Survey of Emission Regions*, *Astrophys. J.* **159** (1970) 379.
- [3] PLANCK collaboration, *Planck 2018 results. VII. Isotropy and Statistics of the CMB*, *Astron. Astrophys.* **641** (2020) A7 [[1906.02552](#)].
- [4] D. Clowe, M. Bradac, A.H. Gonzalez, M. Markevitch, S.W. Randall, C. Jones et al., *A direct empirical proof of the existence of dark matter*, *Astrophys. J. Lett.* **648** (2006) L109 [[astro-ph/0608407](#)].
- [5] G.R. Blumenthal, S.M. Faber, J.R. Primack and M.J. Rees, *Formation of Galaxies and Large Scale Structure with Cold Dark Matter*, *Nature* **311** (1984) 517.
- [6] C.J. Copi, D.N. Schramm and M.S. Turner, *Big bang nucleosynthesis and the baryon density of the universe*, *Science* **267** (1995) 192 [[astro-ph/9407006](#)].
- [7] L.B. Okun, *Limits of Electrodynamics: Paraphotons*, *Sov. Phys. JETP* **56** (1982) 502.
- [8] B. Holdom, *Two U(1)'s and Epsilon Charge Shifts*, *Phys. Lett. B* **166** (1986) 196.
- [9] J. Preskill, M.B. Wise and F. Wilczek, *Cosmology of the Invisible Axion*, *Phys. Lett. B* **120** (1983) 127.

- [10] C.P. Burgess, M. Pospelov and T. ter Veldhuis, *The Minimal model of nonbaryonic dark matter: A Singlet scalar*, *Nucl. Phys. B* **619** (2001) 709 [[hep-ph/0011335](#)].
- [11] S.S. Chakrabarty and I. Jaeglé, *Search for dark photon, axion-like particles, dark scalar, or light dark matter in Compton-like processes*, [1903.06225](#).
- [12] L. Su, L. Wu and B. Zhu, *Probing for an ultralight dark photon from inverse Compton-like scattering*, *Phys. Rev. D* **105** (2022) 055021 [[2105.06326](#)].
- [13] S. Wang, C. Fu, D.-C. Dai, H. Wang, G. Fan, X. Cao et al., *Searching for dark matter particles using Compton scattering*, *Chin. Phys. C* **45** (2021) 093001 [[2107.07584](#)].
- [14] S.C. İnan and A.V. Kisselev, *Search for invisible dark photon in γe scattering at future lepton colliders*, *Eur. Phys. J. C* **82** (2022) 592 [[2112.13070](#)].
- [15] C.P. Oliveira, D. Hadjimichef and M.V.T. Machado, *Compton-like dark photon production in electron–nucleus collisions*, *J. Phys. G* **49** (2022) 035001.
- [16] L. Liu et al., *Status of SIRIUS operation with users*, *JACoW IPAC2023* (2023) WEOGA2.
- [17] M. Alves and F. de Sá, *Beam-based characterization of longitudinal coupled-bunch instabilities at SIRIUS storage ring*, *JACoW IPAC2025* (2025) WEPM104.
- [18] B. Holdom, *Two $U(1)$'s and ε charge shifts*, *Physics Letters B* **166** (1986) 196.
- [19] A. Filippi and M. De Napoli, *Searching in the dark: the hunt for the dark photon*, *Reviews in Physics* **5** (2020) 100042.
- [20] M. Fabbrichesi, E. Gabrielli and G. Lanfranchi, *The Physics of the Dark Photon: A Primer*, Springer International Publishing (2021), [10.1007/978-3-030-62519-1](#).
- [21] R.E. et al., *Dark sectors and new, light, weakly-coupled particles*, 2013.
- [22] E.C.G. Stueckelberg, *Interaction forces in electrodynamics and in the field theory of nuclear forces*, *Helv. Phys. Acta* **11** (1938) 299.
- [23] H. RUEGG and M. RUIZ-ALTABA, *The stueckelberg field*, *International Journal of Modern Physics A* **19** (2004) 3265–3347.
- [24] K. Nakayama and W. Yin, *Hidden photon and axion dark matter from symmetry breaking*, *Journal of High Energy Physics* **2021** (2021) .
- [25] J. Redondo and A. Ringwald, *Light shining through walls*, *Contemporary Physics* **52** (2011) 211–236.
- [26] A.A. Anselm, *Arion \leftrightarrow Photon Oscillations in a Steady Magnetic Field. (In Russian)*, *Yad. Fiz.* **42** (1985) 1480.
- [27] K. Van Bibber, N.R. Dagdeviren, S.E. Koonin, A. Kerman and H.N. Nelson, *Proposed experiment to produce and detect light pseudoscalars*, *Phys. Rev. Lett.* **59** (1987) 759.
- [28] D.F.J.K.K. van Bibber, *The Search for Ultralight Bosonic Dark Matter*, Springer Cham (2022), <https://doi.org/10.1007/978-3-030-95852-7>.
- [29] J. Redondo, *Helioscope bounds on hidden sector photons*, *Journal of Cosmology and Astroparticle Physics* **2008** (2008) 008.
- [30] K. Ehret, M. Frede, S. Ghazaryan, M. Hildebrandt, E.-A. Knabbe, D. Kracht et al., *New alps results on hidden-sector lightweights*, *Physics Letters B* **689** (2010) 149.

- [31] M. Betz, F. Caspers, M. Gasior, M. Thumm and S.W. Rieger, *First results of the cern resonant weakly interacting sub-ev particle search (crows)*, *Phys. Rev. D* **88** (2013) 075014.
- [32] A. Romanenko, R. Harnik, A. Grassellino, R. Pilipenko, Y. Pischalnikov, Z. Liu et al., *Search for dark photons with superconducting radio frequency cavities*, *Phys. Rev. Lett.* **130** (2023) 261801.
- [33] J. Frerick, F. Kahlhoefer and K. Schmidt-Hoberg, *A' view of the sunrise: boosting helioscopes with angular information*, *Journal of Cosmology and Astroparticle Physics* **2023** (2023) 001.
- [34] T. O'Shea, M. Giannotti, I. Irastorza, L. Plasencia, J. Redondo, J. Ruz et al., *Prospects on the detection of solar dark photons by the international axion observatory*, *Journal of Cosmology and Astroparticle Physics* **2024** (2024) 070.
- [35] S.R. Parker, J.G. Hartnett, R.G. Povey and M.E. Tobar, *Cryogenic resonant microwave cavity searches for hidden sector photons*, *Phys. Rev. D* **88** (2013) 112004.
- [36] M. Betz and F. Caspers, *A microwave paraphoton and axion detection experiment with 300 db electromagnetic shielding at 3 ghz*, 2012.
- [37] T. Inada, T. Namba, S. Asai, T. Kobayashi, Y. Tanaka, K. Tamasaku et al., *Results of a search for paraxphotons with intense x-ray beams at spring-8*, *Physics Letters B* **722** (2013) 301.
- [38] R.G. Povey, J.G. Hartnett and M.E. Tobar, *Microwave cavity light shining through a wall optimization and experiment*, *Phys. Rev. D* **82** (2010) 052003.
- [39] M. Schwarz, E.-A. Knabbe, A. Lindner, J. Redondo, A. Ringwald, M. Schneide et al., *Results from the solar hidden photon search (ships)*, *Journal of Cosmology and Astroparticle Physics* **2015** (2015) 011.
- [40] M. Danilov, S. Demidov and D. Gorbunov, *Constraints on hidden photons produced in nuclear reactors*, *Phys. Rev. Lett.* **122** (2019) 041801.
- [41] P. Sikivie, *Experimental tests of the "invisible" axion*, *Phys. Rev. Lett.* **51** (1983) 1415.
- [42] D.F. Bartlett, P.E. Goldhagen and E.A. Phillips, *Experimental test of coulomb's law*, *Phys. Rev. D* **2** (1970) 483.
- [43] J. Jaeckel and S. Roy, *Spectroscopy as a test of coulomb's law: A probe of the hidden sector*, *Physical Review D* **82** (2010) .
- [44] D. Kroff and P. Malta, *Constraining hidden photons via atomic force microscope measurements and the plimpton-lawton experiment*, *Physical Review D* **102** (2020) .
- [45] R.H. Hadfield, *Single-photon detectors for optical quantum information applications*, *Nature Photonics* **3** (2009) 696.
- [46] K.D. Shah, J. Zhou, J. Roper, A. Dhakaan, H. Al-Hallaq, A. Pourmorteza et al., *Photon-counting ct in cancer radiotherapy: Technological advances and clinical benefits*, 2024.
- [47] B. Kreisler, *Photon counting detectors: Concept, technical challenges, and clinical outlook*, *European Journal of Radiology* **149** (2022) 110229.
- [48] *Parâmetros do anel de armazenamento do laboratório nacional de luz síncrotron*, November 13th, 2024.
- [49] S.D. Cova and M. Ghioni, *Single-photon counting detectors*, *IEEE Photonics Journal* **3** (2011) 274.

- [50] R. Klanner, *Characterisation of sipms*, *Nuclear Instruments and Methods in Physics Research Section A: Accelerators, Spectrometers, Detectors and Associated Equipment* **926** (2019) 36.
- [51] S. Ceravolo et al., *X-ray spectroscopy with a photon-counting SiPM-based scintillation detector*, *JINST* **18** (2023) T09007.
- [52] V. Kumar and Z. Luo, *A review on x-ray excited emission decay dynamics in inorganic scintillator materials*, *Photonics* (2021) .
- [53] T. YANAGIDA, *Inorganic scintillating materials and scintillation detectors*, *Proceedings of the Japan Academy, Series B* **94** (2018) 75.
- [54] P.A. Rodnyi, *Physical Processes in Inorganic Scintillators*, CRC Press (2020).
- [55] A. Cemmi, A. Colangeli, B. D'orsi, I. Di Sarcina, E. Diociaiuti, S. Fiore et al., *Radiation study of lead fluoride crystals*, *Journal of Instrumentation* **17** (2022) T05015.
- [56] S. Bertelli et al., *Beam diagnostics with silicon pixel detector array at PADME experiment*, *JINST* **19** (2024) C01016.
- [57] S. Nievaart, B. Janssen and R. Middendorp, *Pairing cdte array detector capabilities with traditional gamma-spectrometry setup for revealing betas in mixed gamma-beta energy spectra for free release measurements*, *Nuclear Instruments and Methods in Physics Research Section A: Accelerators, Spectrometers, Detectors and Associated Equipment* **1078** (2025) 170643.
- [58] G. Deptuch, J. Berst, G. Claus, C. Colledani, W. Dulinski, U. Goerlach et al., *Design and testing of monolithic active pixel sensors for charged particle tracking*, in *2000 IEEE Nuclear Science Symposium. Conference Record (Cat. No.00CH37149)*, vol. 1, pp. 3/41–3/48 vol.1, 2000, DOI.
- [59] R. Turchetta, *CMOS monolithic active pixel sensors (MAPS) for scientific applications*, .
- [60] I. Peric, *A novel monolithic pixel detector implemented in high-voltage cmos technology*, in *2007 IEEE Nuclear Science Symposium Conference Record*, vol. 2, pp. 1033–1039, 2007, DOI.
- [61] M. Carena, J. Osborne, N.R. Shah and C.E.M. Wagner, *Return of the wimp: Missing energy signals and the galactic center excess*, *Phys. Rev. D* **100** (2019) 055002.
- [62] A. Canepa, *Searches for supersymmetry at the large hadron collider*, *Reviews in Physics* **4** (2019) 100033.
- [63] M. Abdughani, K.-i. Hikasa, L. Wu, J.M. Yang and J. Zhao, *Testing electroweak susy for muon g-2 and dark matter at the lhc and beyond*, *Journal of High Energy Physics* **2019** (2019) .
- [64] I.F. Ginzburg, G.L. Kotkin, V.G. Serbo and V.I. Telnov, *Colliding gamma e and gamma gamma Beams Based on the Single Pass Accelerators (of Vlepp Type)*, *Nucl. Instrum. Meth.* **205** (1983) 47.
- [65] P. Sikivie, D.B. Tanner and Y. Wang, *Axion detection in the milli-eV mass range*, *Phys. Rev. D* **50** (1994) 4744 [[hep-ph/9305264](#)].
- [66] K. Homma, T. Hasebe and K. Kume, *The first search for sub-eV scalar fields via four-wave mixing at a quasi-parallel laser collider*, *PTEP* **2014** (2014) 083C01 [[1405.4133](#)].
- [67] T. Hasebe, K. Homma, Y. Nakamiya, K. Matsuura, K. Otani, M. Hashida et al., *Search for sub-eV scalar and pseudoscalar resonances via four-wave mixing with a laser collider*, *PTEP* **2015** (2015) 073C01 [[1506.05581](#)].

- [68] K. Homma, F. Ishibashi, Y. Kirita and T. Hasada, *Sensitivity to Axion-like Particles with a Three-Beam Stimulated Resonant Photon Collider around the eV Mass Range*, *Universe* **9** (2023) 20 [[2212.13012](#)].
- [69] W. Chao, Y. Gao, M.-J. Jin, X.-S. Liu and X.-L. Sun, *Probing Sub-eV Dark Photon, Scalar and Axion-like Particle Dark Matters with Transmon Qubits*, *Phys. Dark Univ.* **50** (2025) 102171 [[2412.20850](#)].
- [70] A. Iwazaki, *A Way of Axion Detection with Mass 10^{-4} - 10^{-3} eV Using Cylindrical Sample with Low Electric Conductivity*, [2510.16746](#).
- [71] K. Bartnick, D. Koester, R.-P. Kudritzki, K. Springmann, S. Stelzl and A. Weiler, *New ultralight scalar particles and the mass–radius relation of white dwarfs – the important role of Sirius B*, *Mon. Not. Roy. Astron. Soc.* **545** (2025) staf1811 [[2510.06312](#)].
- [72] J.R. Alves, M. Lindner, F.S. Queiroz and M.S. Vasconcelos, *Search for Axions and Dark Photons Using Single Molecule Magnets*, [2601.01043](#).